Check for updates

Original Research Article

Green Synthesized Reduced Graphene Oxide–Silver Nanocomposite as an Effective Anti-bacterial Agent Towards Chronic Suppurative Otitis Media Pathogens

Pharmacognosy Magazine
22(4) 1575–1586, 2026
© The Author(s) 2026
Article reuse guidelines:
in.sagepub.com/journals-permissions-india
DOI: 10.1177/09731296261450790
journals.sagepub.com/home/phm
Sage

Lizhu Wang[1], Yanli Yang[2], Shuling Li[2] and Biao Ruan[2]

Abstract

Background: Chronic suppurative otitis media (CSOM) is a significant cause of hearing impairment in developing countries and is frequently associated with severe intracranial and extracranial complications. The increasing prevalence of antibiotic-resistant bacterial strains in CSOM cases underscores the urgent requirement for innovative and effective therapeutic strategies. The World Health Organization (WHO) has estimated that approximately 80% of individuals in low-resource countries rely on traditional medicine to satisfy their primary healthcare needs, emphasizing the potential value of plant-based remedies in addressing such infections.

Materials and Methods: The current study primarily focused on the green synthesis of Reduced graphene oxide–silver nanocomposites (rGO/Ag NCs) using *Cleome viscosa* leaf extract. Characterization was carried out using various spectroscopic techniques, and anti-microbial activity was evaluated *in vitro* using the disc diffusion method. The significant role of microbial agents in the etiology of CSOM was underscored by the confirmation of bacterial infections in 79 (61.7%) of the 128 patient-derived samples analyzed. The predominance of drug-resistant strains was revealed through standardized methods for bacterial isolation and identification, underscoring the urgent need for innovative and effective anti-microbial therapies.

Results: The synthesized nanocomposites were characterized using spectroscopic techniques, which showed a consistent dimension of approximately 20 nm and a uniform distribution of AgNPs on graphene sheets, as evidenced by the surface plasmon resonance (SPR) peak at approximately 420 nm. The anti-microbial activity of the rGO/Ag NCs was evaluated using the disc diffusion method, which resulted in inhibition zones measuring 12.85 ± 0 mm for *Staphylococcus aureus* and 14.08 ± 0 mm for *Pseudomonas aeruginosa*. The rGO/Ag NCs demonstrated superior anti-bacterial activity against multidrug-resistant microorganisms that are associated with CSOM. Furthermore, the experimental groups did not exhibit any significant differences in body weight, food consumption, or hydration intake, which suggests high biocompatibility and systemic stability.

Conclusion: The rGO/Ag NCs demonstrated effective anti-microbial properties and did not exhibit any signs of acute or sub-acute toxicity, highlighting their potential as a therapeutic choice for the treatment of CSOM and other associated ear infections.

Keywords

Chronic suppurative otitis media, reduced graphene oxide–silver nanocomposites, anti-microbial, toxicity

Received 06 January 2025; **revised** 10 September 2025; **accepted** 02 April 2026

Introduction

An inflammatory condition that manifests with or without an intact tympanic membrane in the middle ear is chronic suppurative otitis media (CSOM). A persistent middle ear infection that typically involves tympanic membrane perforation and persists for more than 3 months is known as CSOM (Kombade et al., 2021). Otitis media is a prevalent condition

[1]Department of Otolaryngology, Affiliated Hospital of Yunnan University, Kunming, Yunnan, China
[2]The First Department of Otolaryngology, The First Affiliated Hospital of Kunming Medical University, Kunming, Yunnan, China

Corresponding author:
Biao Ruan, The First Department of Otolaryngology, The First Affiliated Hospital of Kunming Medical University, 295 Xichang Road, Kunming, Yunnan 650032, China.
E-mail: biaoruan00@outlook.com

Creative Commons Non Commercial CC BY-NC: This article is distributed under the terms of the Creative Commons Attribution-NonCommercial 4.0 License (http://www.creativecommons.org/licenses/by-nc/4.0/) which permits non-Commercial use, reproduction and distribution of the work without further permission provided the original work is attributed as specified on the SAGE and Open Access pages (https://us.sagepub.com/en-us/nam/open-access-at-sage).

in children worldwide and is a significant contributor to the prescription of antibiotics (Mahdiani et al., 2021). Particularly in pediatric groups, this disorder has a significantly elevated incidence. The high rate of CSOM in developing regions has been increased by factors such as inadequate nutrition, poor sanitation, and limited health awareness. The World Health Organization (WHO) estimates that CSOM impacts between 65 and 330 million individuals globally, with approximately 60% of those affected experiencing hearing loss. Furthermore, the incidence rate is estimated to be 9 cases per 100,000 individuals (Mahdiani et al., 2021).

CSOM is the result of the presence of infectious agents. *Pseudomonas aeruginosa*, *Staphylococcus aureus*, *Proteus*, and *Klebsiella* species are the most frequently encountered pathogens associated with CSOM. Polymicrobial infections are common, frequently involving anaerobic bacteria, and new pathogenic flora may arise when the defenses of the external auditory canal are compromised (Kombade et al., 2021). Fortunately, the probability of otitis media developing into a life-threatening condition has been substantially reduced by improvements in antibiotic therapies and diagnostic methods. Recent research has shown that antibiotics are ineffective in counteracting the progression of CSOM, even in high-risk pediatric groups (Mahdiani et al., 2021). In instances of CSOM, secondary fungal infections may arise when the ear discharge fails to respond to antibiotic ear drops (Kaur et al., 2022).

The use of phytochemicals in green synthesis provides a sustainable and cost-effective alternative to produce large-scale nanomaterials. This method is chemically complex, yet environmentally benign. In the synthesis of nanoparticles, plant extracts function as efficient reducing and capping agents. In contrast to conventional physical and chemical synthesis methods, phytochemical-based bio-reduction enables the production of nanomaterials that are highly stable, dispersible, and environmentally benign. These nanomaterials are particularly well-suited for biomedical applications due to their non-toxic synthesis processes (Iravani, 2011). The use of non-hazardous materials, the production of safe refuse, reduced processing efforts, and reproducibility are also advantages of green synthesis (Varma, 2012). In recent years, several studies have investigated the anti-microbial potential of rGO/Ag NCs by employing biogenic synthesis methodologies with plant and fungal extracts (de Faria et al., 2014; Sedki et al., 2015; Upadhyay et al., 2015).

Cleome viscosa Linn., also known as "wild or dog mustard," is a sticky annual herb from the Capparaceae family. It is a common weed that is extensively distributed throughout the plains of India and tropical regions worldwide. *C. viscosa* has been traditionally used to treat ear infections and has been shown to possess broad-spectrum anti-microbial activity against pathogens associated with otitis media. Recent research has further substantiated its efficacy as a promising herb for treating otitis media, and numerous studies have validated its anti-microbial effectiveness. The results indicate that *C. viscosa* extracts are effective in treating otitis media, a characteristic that is attributed to their strong anti-microbial properties (Jane & Patil, 2012).

Therefore, the present study aims to synthesize and characterize reduced graphene oxide–silver nanocomposites (rGO/Ag NCs) using *C. viscosa* leaf extract via a green synthesis approach, and to evaluate their *in vitro* anti-bacterial efficacy against multidrug-resistant bacterial strains associated with CSOM. The objective of this research is to evaluate the nanocomposite's potential as a novel therapeutic choice for the treatment of chronic ear infections and to study its synergistic anti-microbial properties.

Materials and Methods

Toxicity Studies

Male and female rats of the Wistar strain, who were 5–8 weeks old and weighing between 110 and 150 g, were acquired from the Experimental Animal Center, Kunming Medical University, Kunming City, Yunnan Province, 650000, China. At ambient temperature, the animals were separately housed in iron cages of 10 × 16 cm, subjected to a 12 h photic–non-photic cycle inside their assigned area. The rats underwent a seven-day acclimatization phase before the trial began.

LD_{50} Assay

The LD_{50} (lethal dose) is a measurement that quantifies the short-term toxicity of a substance by determining the dose of a drug or extract that causes the mortality of 50% of the test animals when administered simultaneously. In accordance with OECD Test Guideline 420 (Acute Oral Toxicity–Fixed Dose Procedure), this guideline recommends a stepwise approach using geometrically spaced dose increments to evaluate potential toxicity while minimizing animal usage. A single oral dose of rGO/Ag NCs was administered to Wistar rats at incremental concentrations of 250, 500, 750, and 1,000 mg/kg body weight for LD_{50} testing. Subsequently, the experimental mice were observed for 72 h (Attanayake et al., 2013).

Collection and Processing of Microbial Samples

The study was conducted after approval from the institutional ethics committee, and written informed consent was taken before recruiting the study participants into the study after giving and explaining to them the participant information sheet in their local language.

Inclusion Criteria

All patients of either sex aged between 15 and 60 years presenting with CSOM and chronic ear discharge, planned for surgery with bacterial infection as per culture results from ear swabs, were included in our study.

Exclusion Criteria

The patients with acute infection of the middle ear with a duration of illness <3 months or patients with a history of traumatic perforations of the eardrum were excluded from this study.

The Institutional Ethical Committee guidelines of the First Affiliated Hospital of Kunming Medical University granted approval for this investigation, which comprised 128 patients who visited the otorhinolaryngology outpatient department. Ear swabs were used to extract pus samples, which were processed within 6 h. At 37°C for 24–48 h, the samples were cultured on blood agar and MacConkey agar plates. Subsequently, the samples were incubated in 2 mL of nutrient broth for an additional 24 h. The results of the cultured dishes were subsequently analyzed and documented. Bacterial identification was made using the Vitek 2 system, biochemical characteristics, and colony morphology.

Anti-bacterial Study

The synthesized rGO, AgNPs, and rGO/Ag NCs were tested against Gram-negative bacteria, *P. aeruginosa*, and Gram-positive bacteria, *S. aureus*, using disc diffusion and broth dilution methods (Fayaz et al., 2010). For anti-bacterial analysis, bacterial cultures were cultivated on Mueller–Hinton (MH) agar and broth.

The samples were evaluated against chloramphenicol, a standard broad-spectrum antibiotic, serving as a positive control for the disc diffusion assay. Plain paper discs served as the negative control. To obtain a concentration of 50 µg per disc, autoclaved samples and chloramphenicol were applied to paper discs using a drop-drying technique. Before being inoculated onto agar plates, the optical density of the bacterial suspensions was adjusted to 0.5 in MH broth. The discs were labeled appropriately (plates were divided into five sections and labeled as follows: rGO, AgNPs, rGO–Ag, chloramphenicol, and plain paper disc), placed on the agar surface, and incubated at 37°C for 24 h. The anti-microbial efficacy of each disc was assessed by measuring the diameter of the inhibition zone located around it.

Statistical Analysis

The results are expressed as mean ± standard deviation (SD). Analysis was done in triplicate, and we used the mean for statistical analysis. One-way analysis of variance (ANOVA) test helps in the determination of statistical significance, followed by a *post hoc* Tukey test. $p < .05$ was the fixed statistical significance.

Results

UV-Spectroscopy

The UV–vis spectra of GO, rGO, and rGO/Ag NCs are shown in Figure 1(A). At 210 nm and 250 nm, the two distinct peak values of GO are the π–π* transitions of aromatic C–C bonds and the *n*–π* transitions of C=O bonds, respectively. The reclamation of the conjugated sp^2 carbon network (de Faria et al., 2014; Li & Liu, 2010; Liu et al., 2010; Yuan, Chai, et al., 2012) is indicated by the appearance of a characteristic band at 250 nm. The surface plasmon resonance (SPR) of AgNPs is indicated by the formation of a new peak at 420 nm, which evidences the incorporation of AgNPs onto the rGO surface (Gurunathan et al., 2009; Li & Liu, 2010; Liu et al., 2010; Xu & Wang, 2009). The disappearance of rGO-specific peaks alongside the appearance of a band related to AgNPs suggests a simultaneous reduction of both rGO and $AgNO_3$, leading to the formation of rGO/Ag NCs.

X-ray Diffraction

The crystalline structure of rGO/Ag NCs was confirmed through the X-ray diffraction (XRD) pattern, as shown in Figure 1(B). GO exhibited a unique reflection at ($2\theta = 10.7°$), which was in stark contrast to the characteristic reflection of pristine graphite at $2\theta = 26.6°$. The graphitic structure in rGO was restored, as evidenced by the disappearance of the GO reflection at $2\theta = 10.7°$ and the emergence of a new reflection at $2\theta = 26.4°$, following reduction. Additional reflections were observed at $2\theta = 33.2°$ and 45.5° in the case of rGO/Ag NCs, which correspond to the (111) and (200) planes of the cubic Ag crystal, respectively, as identified using JCPDS No. 04-0783 (Baba et al., 2009; Hu et al., 2013; Li & Liu, 2010; Zhang et al., 2011; Zhou et al., 2009).

Fourier Transform Infrared

The Fourier transform infrared (FTIR) spectra of rGO/Ag NCs, rGO, and GO are shown in Figure 1(C). Distinct peaks are identified in the GO spectrum at 1,018, 1,198, 1,345, 1,585, 1,698, and 3,390 cm^{-1}. The stretching vibrations of C–O–C bonds in epoxy or alkoxy groups are represented by the peak at 1,018 cm^{-1}. The peak at 1,198 cm^{-1}, which is attributed to C–OH bonds, and the band at 1,585 cm^{-1}, which represents C=C bonds, are indicative of skeletal vibrations in unoxidized graphite regions. The peak at 1,698 cm^{-1} is indicative of the presence of C=O bonds in carboxylic acids and carbonyl compounds (Gurunathan et al., 2013; Marcano et al., 2010; Zuo et al., 2013). In addition, the absorption band at 1,585 cm^{-1} is linked to C=C bonds in aromatic rings within the GO carbon framework (Gurunathan et al., 2014). The successful assimilation of functional groups during the interaction between CVE, rGO, and Ag components is indicated by the appearance of a new band at 1,415 cm^{-1} in the rGO/Ag NC spectrum, which is attributed to C–N stretching vibrations. This attribute confirms the effective preparation of rGO/Ag NCs. Compared to GO, the intensity of peaks at 1,080, 1,265, 1,585, and 3,390 cm^{-1} is significantly diminished, indicating that the functional groups have been modified. Furthermore, an absorption band at 1,585 cm^{-1} is

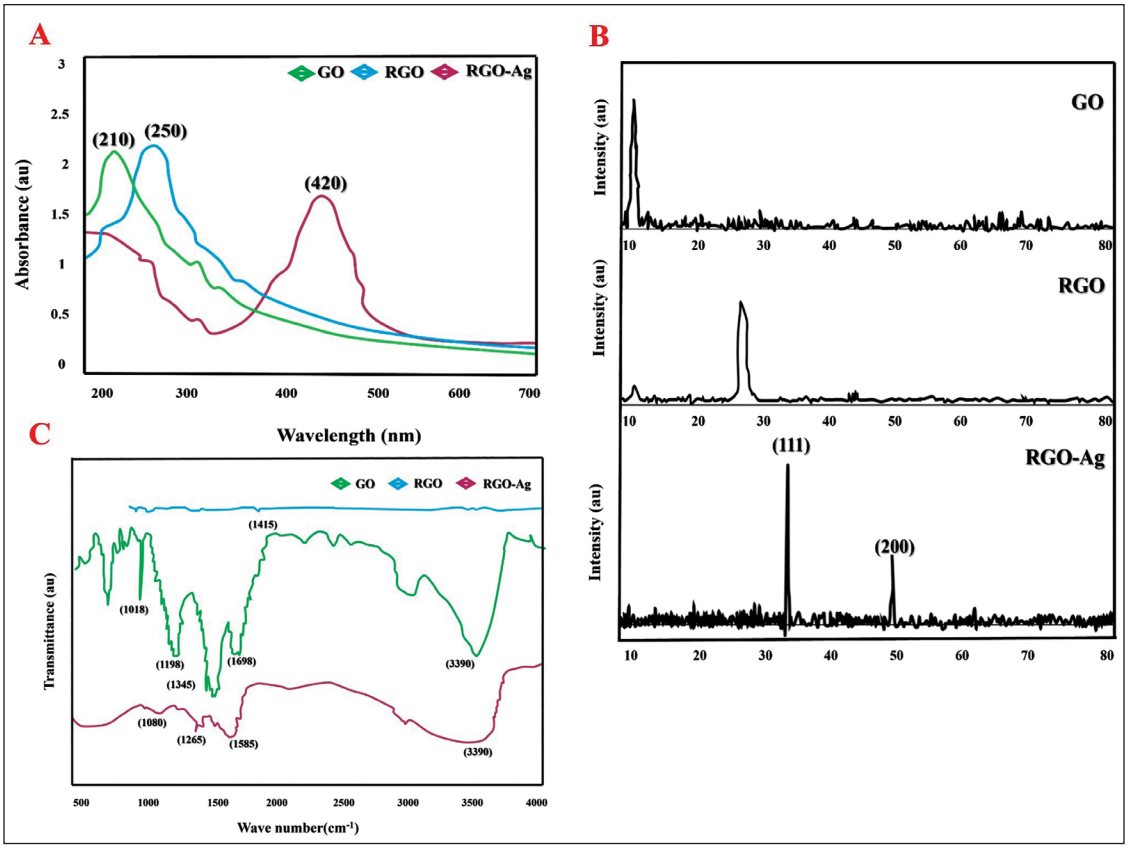


Figure 1. (A) UV–Visible Spectra of GO, rGO, and rGO/Ag NCs Synthesized Using Leaf Extract of *Cleome viscosa.* (B) X-ray Diffraction (XRD) Analysis of GO, rGO, and rGO/Ag NCs Synthesized Using Leaf Extract of *Cleome viscosa*. (C) Fourier Transform Infrared (FTIR) Spectra of GO, rGO, and rGO/Ag NCs Synthesized Using *C. viscosa*.

identified, which is associated with the skeletal vibrations of graphene sheets.

Transmission Electron Microscopy

The morphological characteristics of GO, rGO, and the rGO/Ag NCs were analyzed using transmission electron microscopy (TEM) and are illustrated in Figure 2(A)–2(C). GO possesses a densely packed, layered, and plate-like structure, as well as a uniform surface, as shown in Figure 2(A). Conversely, rGO (Figure 2(B)) demonstrates a conventional sheet-like structure that is approximately 50 nm in size. Nanoparticles are uniformly anchored to the surface of the rGO sheets in the rGO/Ag NC (Figure 2(C)). Most of these nanoparticles have a diameter of approximately 25 nm and exhibit spherical morphologies, with an even and homogeneous distribution on the rGO surfaces. Furthermore, the TEM images demonstrate that the rGO sheets have silky, wavy structures, which aid in the homogeneous dispersion of the AgNPs. The rGO sheets are uniformly distributed with AgNPs that are well-dispersed, with a consistent dimension of approximately 20 nm. The smooth, elegant, and undulating configuration of the rGO/Ag NC probably serves an essential function in inhibiting nanoparticle clustering and ensuring a surface that supports the consistent bonding of AgNPs to the graphene sheets.

Selected Area Electron Diffraction

Figure 2(D) illustrates selected area electron diffraction (SAED) images of the rGO/Ag NCs. Two distinct regions were identified: A light gray area that corresponds to rGO and a darker gray region that represents AgNPs. The interplanar spacing of FCC-structured silver was measured at 0.235 nm in Figure 2(D), which corresponds to the (111) plane. Furthermore, the formation of polycrystalline rGO/Ag NCs was evident in Figure 2(D), as evidenced by the distinct observation of diffraction rings corresponding to the (111), (200), (220), and (311) planes.

Raman Spectroscopy

The Raman spectra of GO and rGO/Ag NCs are illustrated in Figure 3. It has been observed that the GO spectra contain a significant D band at 1,340 cm^{-1}. This band corresponds to the respiration mode of A1g symmetry. In addition, the G band is indicated by a peak at approximately 1,602 cm^{-1}, which is the result of the first-order scattering of the E2g phonon of sp^2-hybridized carbon atoms. Following the *in situ* reduction of

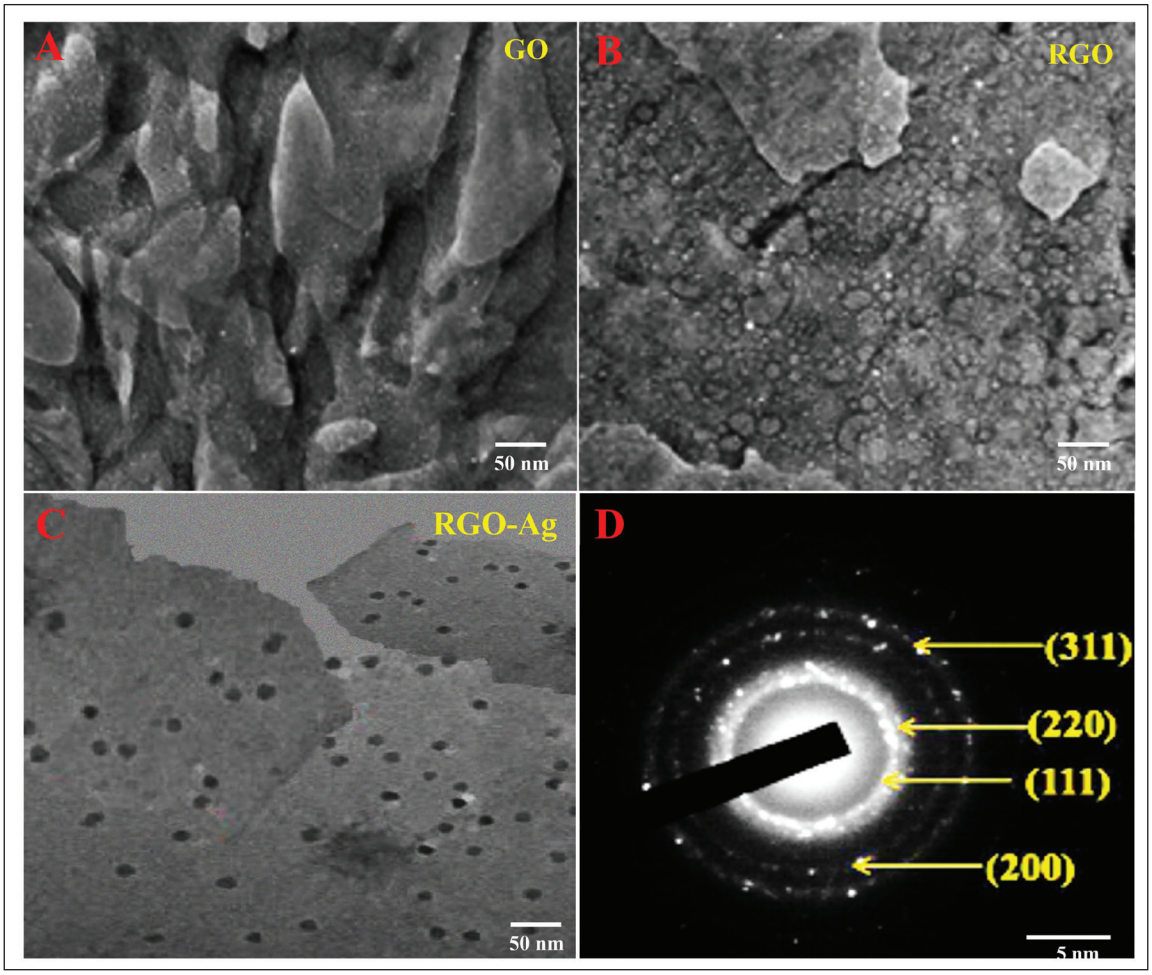


Figure 2. Transmission Electron Microscopy (TEM) Images of (A) GO, (B) rGO, and (C) rGO/Ag NCs. (D) Selected Area Electron Diffraction (SAED) Pattern of rGO/Ag NCs.

GO sheets and Ag ions to form rGO/Ag NCs, substantial modifications to the Raman spectra are observed. In contrast, the strength of the G band undergoes a significant increase, while the strength of the D band decreases. Furthermore, the peaks in the rGO/Ag NC spectrum are more pronounced than those in GO, suggesting that the structural ordering is improved. The G band of rGO/Ag NCs also slightly shifts from its position at approximately 1,602 cm^{-1} in GO, indicating a greater degree of restoration of the hexagonal carbon network that is a characteristic of the reduction of GO to rGO. The transformation from GO to rGO and the successful incorporation of Ag nanoparticles are further emphasized by the relationship between the D band strength and in-plane sp^2 domain size, which further emphasizes the structural changes induced by the reduction process (Tian et al., 2014).

Isolation and Identification of a Bacteriological Sample

The causative organisms were identified by enrolling 128 patients with ear infections in this study. Of these, 74 patients were from urban areas, and 54 were from rural areas. The diagnosis revealed that 79 patients had CSOM. The study confirmed that ear infections occur across a wide age range by including patients from all age categories.

In order to investigate colony morphology, ear probe samples were cultured on a variety of agar media. Single colonies were identified in 105 samples, while no microbial growth was observed in 11 samples (8.59%). Microbial growth was observed in 117 of the 128 ear discharge samples. Eight samples exhibited double colonies, while four samples exhibited three or more colonies. Of the 117 colonies, 82.03% were single colonies.

Toxicity

In the 72 h period following the administration of rGO/Ag NCs, the animal groups did not exhibit any indications of toxicity in response to doses of 250, 500, 750, and 1,000 mg/kg in the LD_{50} experiment. The treated and control groups did not exhibit any significant differences in biochemical blood markers and organ function assays, as summarized in Table 1.

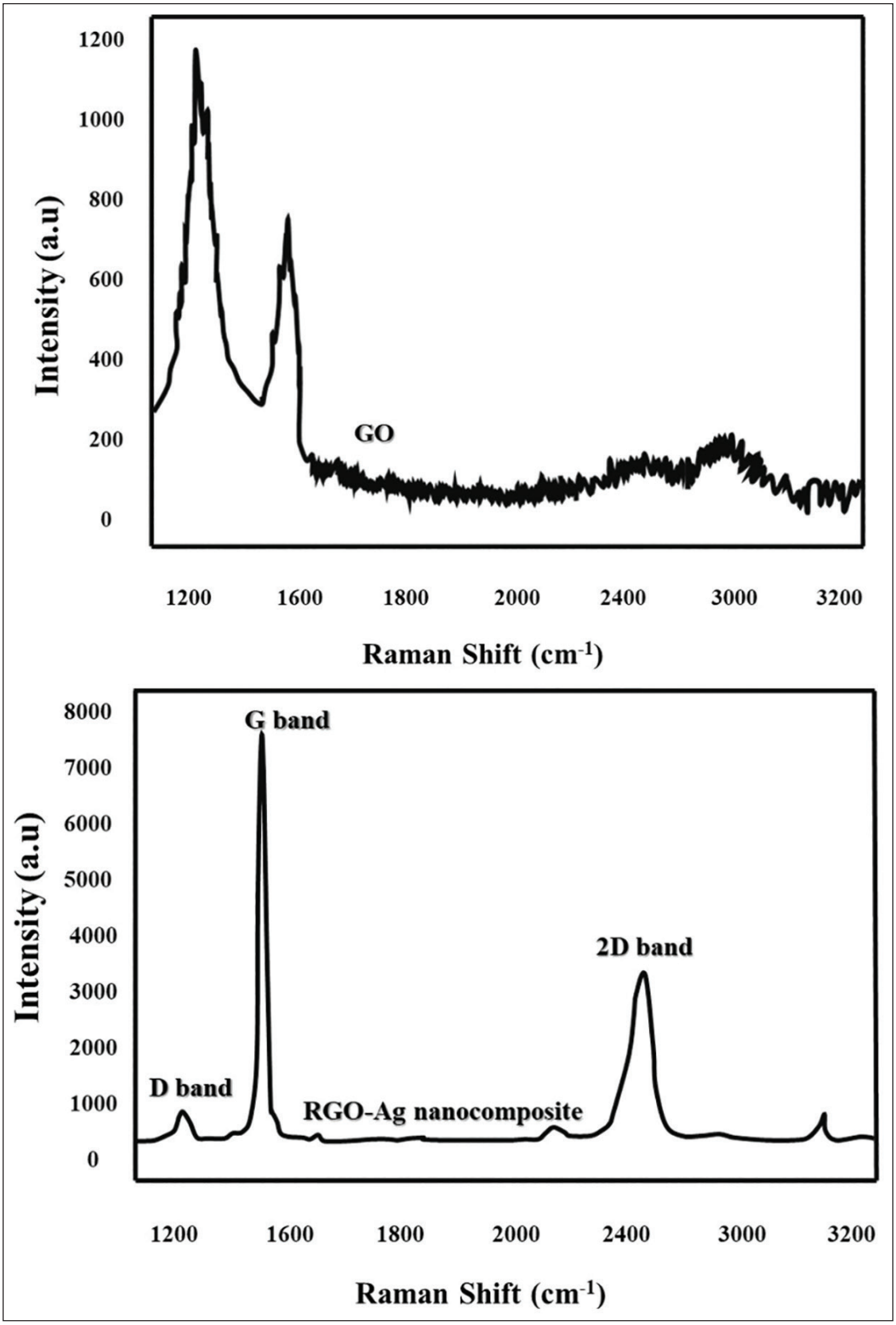


Figure 3. Raman Spectra of GO, rGO, and rGO/Ag NCs Synthesized Using *Cleome viscosa*.

Table 1. Biological Indices and Typical Behavioral Patterns Assessed in Toxicity Study.

	Dose (mg/kg)				
Type of Behavior	**Control**	**250**	**500**	**750**	**1,000**
Alertness	Normal	Normal	Normal	Normal	Normal
Awareness	Normal	Normal	Normal	Normal	Normal
Voluntary reaction	Normal	Normal	Normal	Normal	Normal
Nociceptive reaction	Normal	Normal	Normal	Normal	Normal
Somatosensory response	Normal	Normal	Normal	Normal	Normal
Acoustic reflex	Normal	Normal	Normal	Normal	Normal
Up righting response	Normal	Normal	Normal	Normal	Normal
Auricular response	Normal	Normal	Normal	Normal	Normal
Forelimb strength	Normal	Normal	Normal	Normal	Normal
Water consumption	Normal	Normal	Normal	Normal	Normal
Feeding behavior	Normal	Normal	Normal	Normal	Normal
Fatality	Normal	Normal	Normal	Normal	Normal

Furthermore, there were no substantial modifications in behavior. Body weight, food, and water intake remained stable across all groups, with no significant variation ($p < .05$) during the dosing regimen. The histological analysis of liver and kidney tissues, as illustrated in Figure 4, verified that the plant extracts did not induce toxicity in these organs.

Anti-microbial Activity

The anti-bacterial properties of the tested materials were demonstrated by the appearance of inhibition zones around the materials applied to the paper discs, which indicated the suppression of bacterial growth in these areas. Figure 5 illustrates the anti-bacterial efficacy of rGO/Ag NCs. In comparison to the standard antibiotic chloramphenicol, inhibition zones of 12.85 ± 0 mm and 14.08 ± 0 mm were observed for *S. aureus* and *P. aeruginosa*, respectively. rGO/Ag NCs demonstrated around twofold the anti-bacterial activity against *S. aureus* and substantially improved efficacy against *P. aeruginosa*, as indicated by disc diffusion analysis. Overall, the nanocomposites demonstrated a nearly 50% inhibition against both bacterial isolates, which was significantly higher than that observed with AgNPs alone ($p < .05$). A detailed summary of the inhibition zone diameters is provided in Table 2.

A comparative analysis of comparable nanomaterial systems was conducted to contextualize this result (Table 3). Upon the addition of modifications, such as hydroxyl, halogen, or aromatic substituents, significant distinctions in anti-bacterial activity become apparent. For example, rGO/Ag NCs functionalized with hydroxyl groups exhibited increased bacterial interaction and enhanced hydrophilicity. In the same vein, halogenated nanocomposites exhibited more potent enzyme-binding affinities, particularly in the presence of Gram-negative strains. Imidazole-based nanocomposites that contain electron-withdrawing groups, such as $–NO_2$, consistently exhibited a more extensive and potent anti-bacterial effect than those that contained electron-donating groups, such as $–CH_3$ or $–OCH_3$ (Al-Marri et al., 2015; Vi et al., 2020).

These findings highlight that the anti-bacterial efficacy of nanomaterials is dependent on their surface chemistry, functional modifications, and elemental composition. Understanding these parameters is indispensable for the strategic development of advanced nanocomposites specifically designed for clinical applications.

Discussion

The present study introduces a sustainable and biocompatible approach for synthesizing rGO/Ag NCs using CVE as a natural reducing and stabilizing agent. Unlike conventional methods that rely on chemical reductants such as ammonia, sodium borohydride, or poly(*N*-vinyl-2-pyrrolidone), the CVE-mediated synthesis operates under neutral pH conditions, eliminating the need for hazardous reagents and offering a greener, safer alternative. This positions the current method as a more accessible and environmentally responsible strategy for nanomaterial fabrication.

The simultaneous reduction of GO and Ag^+ ions by CVE was confirmed through UV–vis spectroscopy, where a SPR band at ~420 nm indicated the formation of AgNPs. This dual reduction mechanism has been previously reported using other plant extracts (Al-Assaly et al., 2025), but the antioxidant-rich profile of CVE appears to enhance the uniformity and stability of the resulting nanocomposite. XRD and FTIR analyses further validated the crystalline nature of AgNPs and the successful reduction of GO, with the

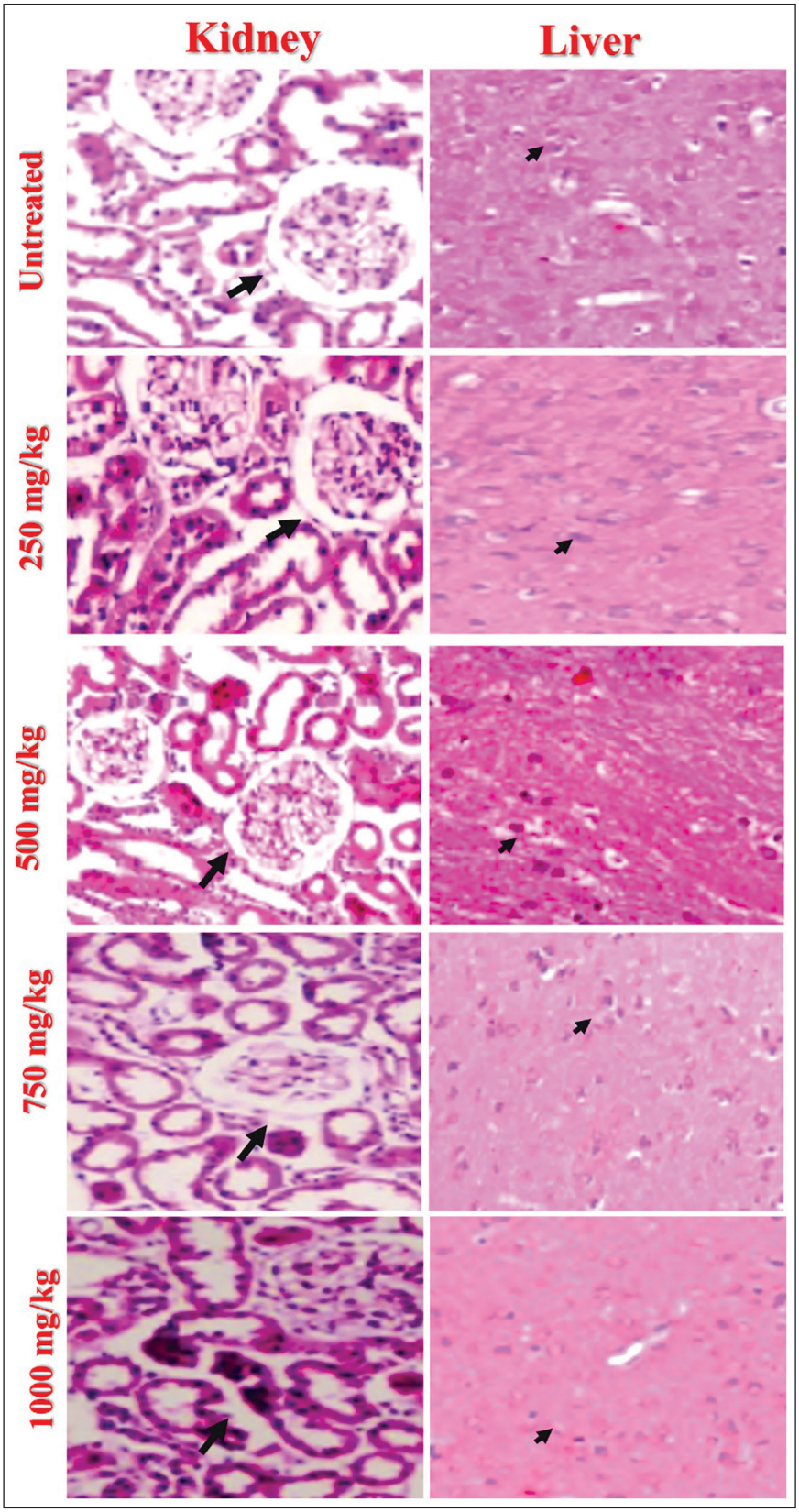


Figure 4. Histology Images of Liver and Kidney Sections Using Hematoxylin and Eosin (H&E) Staining.

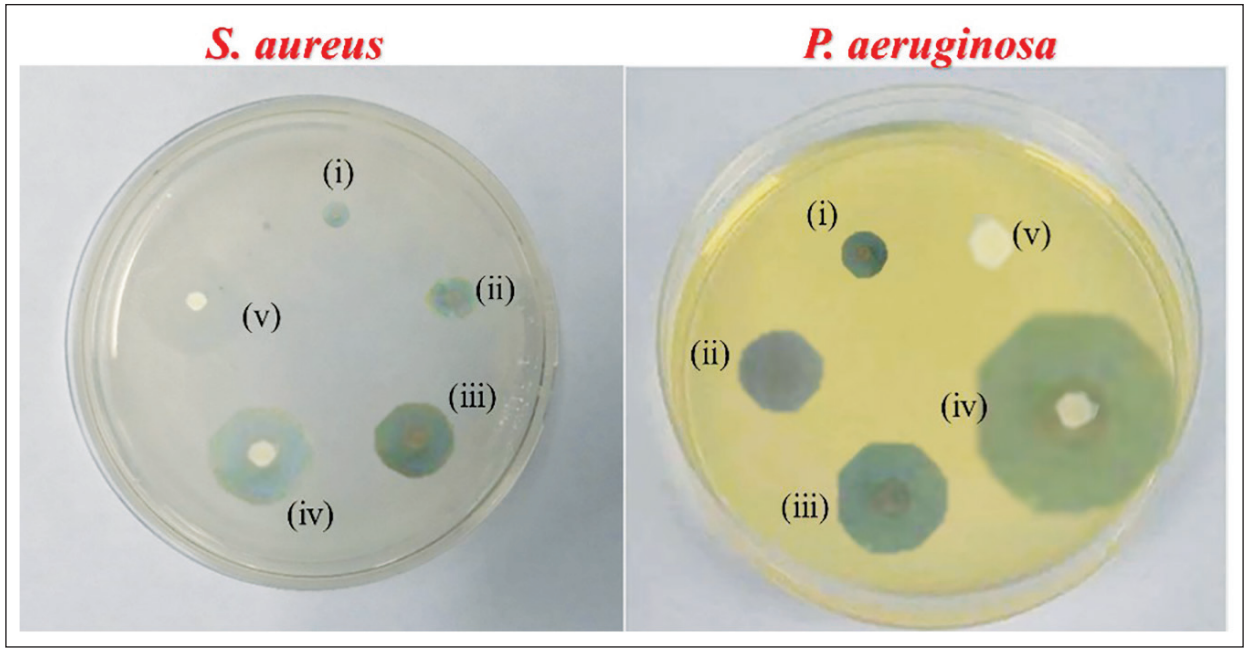


Figure 5. Anti-bacterial Activity of rGO (i), AgNPs (ii), rGO/Ag NC (iii), Chloramphenicol (iv), and Negative Control (v) Against (A) *Staphylococcus aureus* and (B) *Pseudomonas aeruginosa*.

Table 2. Zone of Inhibition Measured for Bacterial Species Using the Disc Diffusion Method.

Name of the Bacteria	rGO	AgNPs	rGO–Ag	Positive Control	Negative Control
Staphylococcus aureus	–	8.98 ± 0.25	12.85 ± 0	26.00 ± 0	–
Pseudomonas aeruginosa	–	5.95 ± 0.26	14.08 ± 0	28.00 ± 0	–

Table 3. Comparative Studies of Substituent Effects on Anti-bacterial Activity in Nanomaterials.

Nanomaterial	Substituents/ Modifications	Tested Pathogens	Efficacy Observed	References
GO–Ag NCs	Unreduced GO with AgNPs	*Staphylococcus aureus*, *Escherichia coli*	Variable: Strain-dependent and less uniform AgNP distribution reduced overall efficacy	Xu et al. (2018)
rGO/Ag (–OH modified)	Hydroxyl groups on rGO	*Pseudomonas aeruginosa*, *Klebsiella pneumoniae*	Increased zone of inhibition and enhanced hydrophilicity and bacterial interaction	Xu et al. (2018)
rGO/Ag (–Cl modified)	Chlorine on AgNP or rGO surface	*Escherichia coli*, *Bacillus subtilis*	Improved Gram-negative activity and EWGs increase bacterial enzyme binding affinity	Xu et al. (2018)
Imidazole-based NCs	Various $–NO_2$, $–CH_3$, $–OCH_3$ groups	*Staphylococcus aureus*, *Enterococcus faecalis*	Substituent-dependent and nitro-substituted compounds showed highest inhibition zones	–
rGO/Ag NCs	No additional modifiers	*Staphylococcus aureus*, *Escherichia coli*, and so on	~50% inhibition strong cooperative effect; no acute or subacute toxicity	–

disappearance of characteristic GO peaks suggesting effective exfoliation and integration of AgNPs into the rGO matrix.

In contrast to GO and rGO, the absence of additional peaks suggested that the reduction of GO and Ag ions was unaffected by other components in the plant extract. The GO peak, which was previously associated with interlamellar water and the clustering of GO layers, vanished following the deposition of AgNPs (Al-Assaly et al., 2025). This indicates that the GO lamellar structure was disrupted during the reduction and incorporation of AgNPs. In comparison to those of GO, the peaks at 1,080, 1,265, 1,585, and 3,390 cm^{-1} in the FTIR spectrum of rGO/Ag NCs are substantially weaker. Previous research on Ag–GO nanocomposites has reported comparable results (Chook et al., 2012).

The TEM analysis demonstrated that the rGO sheets were uniformly and densely coated with AgNPs, with a size of approximately 50 nm. In the same vein, Yuan, Gu, et al. (2012) used an environmentally friendly approach to synthesize graphene–Ag nanocomposites (GNS–AgNPs). They utilized GO as the graphene precursor, $AgNO_3$ as the AgNP precursor, and sodium citrate as both a reducing and stabilizing agent. The resulting AgNPs were deposited on GO sheets. In the current study, the rGO/Ag NCs exhibited transparent and uniform rGO sheets that were densely coated with AgNPs. These AgNPs were wrapped within the rGO structure, and silk-like patterns were observed. These results show that an analogous process has been observed in the synthesis of rGO/Ag NCs, where CVE extracts are essential for promoting reactions among silver and GO (Yuan, Gu, et al., 2012). The Raman spectroscopy results corroborate these findings, as evidenced by comparable observations reported by Xu et al. (2018) in a study that integrated electrical characterization.

rGO/Ag NCs exhibited approximately 50% of the antibacterial activity against the tested pathogens, highlighting their potential for use in anti-bacterial applications. Furthermore, in a similar study involving GO–Ag nanocomposite, both *S. aureus* and *Escherichia coli* demonstrated different anti-bacterial responses (Yuan, Gu, et al., 2012). The rGO/Ag NC did not show any sign of acute or subacute toxicity, and no mortality was observed during the LD_{50} experiment. The cooperative effect of rGO/Ag NC was noticeable, as its overall efficacy exceeded the total impact of the individual contributions of each component. This innovative formulation has the potential to significantly contribute to the development of new treatments for infectious diseases, with a particular emphasis on the management of ear infections, such as CSOM.

Conclusion

This study shows the environmentally friendly synthesis of rGO/Ag NCs and underscores their potential as effective antimicrobial agents against microorganisms responsible for CSOM. The anti-microbial efficacy of rGO/Ag NCs was substantially increased compared to that of rGO or AgNPs alone. The specific toxicity of rGO/Ag NCs against specified bacterial species was confirmed by the disc diffusion method. The rGO/Ag NCs showed approximately 50% of the antimicrobial efficacy of the broad-spectrum antibiotic chloramphenicol against the tested pathogens. These results emphasize the ability of rGO/Ag NCs to be used in anti-bacterial applications and their potential as advanced nanomaterials for the management of infectious diseases, particularly in the treatment of ear infections like CSOM.

However, the present findings are based solely on *in vitro* assays, and *in vivo* validation is essential to confirm therapeutic effectiveness and safety in biological systems. Potential cytotoxicity to human tissues remains unexplored, and long-term stability and resistance development were not assessed. Addressing these limitations, future studies should focus on addressing these aspects through *in vivo* testing, comprehensive toxicological analysis, and extended microbial spectrum evaluation.

Abbreviations

C. viscosa: *Cleome viscosa*; CSOM: Chronic suppurative otitis media; rGO/AG NCs: Reduced graphene oxide–silver nanocomposites; SPR: Surface plasmon resonance.

Acknowledgments

The authors are thankful to the First Affiliated Hospital of Kunming Medical University for providing a platform to do this research.

Declaration of Conflicting Interests

The authors declared no potential conflicts of interest with respect to the research, authorship, and/or publication of this article.

Ethical Approval

This research was carried out in line with the principles and standards outlined in the Institutional Committee on Ethics of Animal Experimentation. All experiments were performed according to ethical committee guidelines of the First Affiliated Hospital of Kunming Medical University (Ethical approval number: 2024. No. 168).

Funding

The authors received no financial support for the research, authorship, and/or publication of this article.

Informed Consent

The study was conducted after approval from the institutional ethics committee, and written informed consent was taken before recruiting the study participants into the study after giving and explaining to them the participant information sheet in their local language.

Supplementary Material

Supplementary material for this article is available online.

ORCID iD

Biao Ruan https://orcid.org/0009-0009-1235-7254

References

Al-Assaly, R., Al-Saigh, R., & Al-Nafiey, A. (2025). Chemically synthesized rGO-Ag NP nanocomposite: Enhanced stability and functionality for biomedical applications. *BioNanoScience*, *15*, 7. https://doi.org/10.1007/s12668-024-01619-2

Al-Marri, A. H., Khan, M., Khan, M., Adil, S. F., Al-Warthan, A., Alkhathlan, H. Z., Tremel, W., Labis, J. P., Siddiqui, M. R. H., & Tahir, M. N. (2015). *Pulicaria glutinosa* extract: A toolbox to synthesize highly reduced graphene oxide–silver nanocomposites. *International Journal of Molecular Sciences*, *16*(1), 1131–1142. https://doi.org/10.3390/ijms16011131

Attanayake, A. P., Jayatilaka, K. A., Pathirana, C., & Mudduwa, L. K. (2013). Efficacy and toxicological evaluation of *Coccinia grandis* (Cucurbitaceae) extract in male Wistar rats. *Asian Pacific Journal of Tropical Disease*, *3*(6), 460–466. https://doi.org/10.1016/S2222-1808(13)60101-2

Baba, T., Convery, P. A., Matsumura, N., Whitaker, R. S., Kondoh, E., Perry, T., Huang, Z., Bentley, R. C., Mori, S., Fujii, S., Marks, J. R., Berchuck, A., & Murphy, S. K. (2009). Epigenetic regulation of *CD133* and tumorigenicity of CD133+ ovarian cancer cells. *Oncogene*, *28*(2), 209–218. https://doi.org/10.1038/onc.2008.374

Chook, S. W., Chia, C. H., Zakaria, S., Ayob, M. K., Chee, K. L., Huang, N. M., Neoh, H. M., Lim, H. N., Jamal, R., & Rahman, R. M. (2012). Antibacterial performance of Ag nanoparticles and AgGO nanocomposites prepared via rapid microwave-assisted synthesis method. *Nanoscale Research Letters*, *7*(1), 541. https://doi.org/10.1186/1556-276X-7-541

de Faria, A. F., Martinez, D. S. T., Meira, S. M. M., de Moraes, A. C. M., Brandelli, A., Souza Filho, A. G., & Alves, O. L. (2014). Anti-adhesion and antibacterial activity of silver nanoparticles supported on graphene oxide sheets. *Colloids and Surfaces B: Biointerfaces*, *113*, 115–124. https://doi.org/10.1016/j.colsurfb.2013.08.006

Fayaz, A. M., Balaji, K., Girilal, M., Yadav, R., Kalaichelvan, P. T., & Venketesan, R. (2010). Biogenic synthesis of silver nanoparticles and their synergistic effect with antibiotics: A study against Gram-positive and Gram-negative bacteria. *Nanomedicine: Nanotechnology, Biology and Medicine*, *6*(1), 103–109. https://doi.org/10.1016/j.nano.2009.04.006

Gurunathan, S., Han, J. W., Park, J. H., & Kim, J. (2014). An *in vitro* evaluation of graphene oxide reduced by *Ganoderma* spp. in human breast cancer cells (MDA-MB-231). *International Journal of Nanomedicine*, *9*(1), 1783–1797. https://doi.org/10.2147/IJN.S57735

Gurunathan, S., Han, J. W., Eppakayala, V., & Kim, J. H. (2013). Microbial reduction of graphene oxide by *Escherichia coli*: A green chemistry approach. *Colloids and Surfaces B: Biointerfaces*, *102*, 772–777. https://doi.org/10.1016/j.colsurfb.2012.09.011

Gurunathan, S., Kalishwaralal, K., Vaidyanathan, R., Venkataraman, D., Pandian, S. R. K., Muniyandi, J., Hariharan, N., & Eom, S. H. (2009). Biosynthesis, purification and characterization of silver nanoparticles using *Escherichia coli*. *Colloids and Surfaces B: Biointerfaces*, *74*(1), 328–335. https://doi.org/10.1016/j.colsurfb.2009.07.048

Hu, C. F., Liu, Y. L., Qin, J. L., Nie, G., Lei, B., Xiao, Y., Zheng, M., & Rong, J. (2013). Fabrication of reduced graphene oxide and silver nanoparticle hybrids for Raman detection of absorbed folic acid: A potential cancer diagnostic probe. *ACS Applied Materials & Interfaces*, *5*(11), 4760–4768. https://doi.org/10.1021/am4000485

Iravani, S. (2011). Green synthesis of metal nanoparticles using plants. *Green Chemistry*, *13*, 2638–2650. https://doi.org/10.1039/C1GC15386B

Jane, R. R., & Patil, S. D. (2012). *Cleome viscosa*: An effective medicinal herb for otitis. *International Journal of Science and Nature*, *3*(1), 153–158.

Kaur, R., Mittal, N., & Sharma, S. (2022). Clinical and microbiological profile of otomycosis in a tertiary care hospital. *International Journal of Otorhinolaryngology and Head and Neck Surgery*, *8*(4), 345–349.

Kombade, S. P., Kaur, N., Patro, S. K., & Nag, V. L. (2021). Clinico-bacteriological and antibiotic drug resistance profile of chronic suppurative otitis media at a tertiary care hospital in Western Rajasthan. *Journal of Family Medicine and Primary Care*, *10*(7), 2572–2579. https://doi.org/10.4103/jfmpc.jfmpc_2480_20

Li, J., & Liu, C. Y. (2010). Ag/graphene heterostructures: Synthesis, characterization and optical properties. *European Journal of Inorganic Chemistry*, *2010*(8), 1244–1248. https://doi.org/10.1002/ejic.200901048

Liu, S., Tian, J. Q., Wang, L., Li, H. L., Zhang, Y. W., & Sun, X. P. (2010). Stable aqueous dispersion of graphene nanosheets: Noncovalent functionalization by a polymeric reducing agent and their subsequent decoration with Ag nanoparticles for enzymeless hydrogen peroxide detection. *Macromolecules*, *43*(23), 10078–10083. https://doi.org/10.1021/ma102230m

Mahdiani, S., Lasminingrum, L., & Anugrah, D. (2021). Management evaluation of patients with chronic suppurative otitis media: A retrospective study. *Annals of Medicine and Surgery*, *67*, 102492. https://doi.org/10.1016/j.amsu.2021.102492

Marcano, D. C., Kosynkin, D. V., Berlin, J. M., Sinitskii, A., Sun, Z., Slesarev, A., Alemany, L. B., Lu, W., & Tour, J. M. (2010). Improved synthesis of graphene oxide. *ACS Nano*, *4*(8), 4806–4814. https://doi.org/10.1021/nn1006368

Sedki, M., Mohamed, M. B., Fawzy, M., Abdelrehim, D. A., & Abdel-Mottaleb, M. M. S. (2015). Phytosynthesis of silver-reduced graphene oxide (Ag-RGO) nanocomposite with an enhanced antibacterial effect using *Potamogeton pectinatus* extract. *RSC Advances*, *5*, 17358–17365. https://doi.org/10.1039/C4RA13117G

Tian, T., Shi, X., Cheng, L., Luo, Y., Dong, Z., & Gong, H. (2014). Graphene-based nanocomposite as an effective multifunctional, and recyclable antibacterial agent. *ACS Applied Materials & Interfaces*, *6*(11), 8542–8548. https://doi.org/10.1021/am5022914

Upadhyay, R. K., Soin, N., Bhattacharya, G., Shah, S., Barman, A., & Roy, S. S. (2015). Grape extract assisted green synthesis of reduced graphene oxide for water treatment application. *Materials Letters*, *160*, 355–358. https://doi.org/10.1016/j.matlet.2015.07.144

Varma, R. S. (2012). Greener approach to nanomaterials and their sustainable applications. *Current Opinion in Chemical Engineering*, *1*(2), 123–128. https://doi.org/10.1016/j.coche.2011.12.002

Vi, T. T. T., Kumar, S. R., Pang, J.-H. S., Liu, Y.-K., Chen, D. W., & Lue, S. J. (2020). Synergistic antibacterial activity of silver-loaded graphene oxide towards *Staphylococcus aureus* and *Escherichia coli*. *Nanomaterials*, *10*(2), 366. https://doi.org/10.3390/nano10020366

Xu, C., & Wang, X. (2009). Fabrication of flexible metal-nanoparticle film using graphene oxide sheets as substrates. *Small*, *5*(19), 2212–2217. https://doi.org/10.1002/smll.200900548

Xu, H. J., Wu, X., Li, X. M., Luo, C., Liang, F., Orignac, E., Zhang, J., & Chu, J. H. (2018). Properties of graphene-metal contacts probed by Raman spectroscopy. *Carbon*, *127*, 491–497. https://doi.org/10.1016/j.carbon.2017.11.035

Yuan, W. H., Gu, Y. J., & Li, L. (2012). Green synthesis of graphene/Ag nanocomposites. *Applied Surface Science*, *261*, 753–758. https://doi.org/10.1016/j.apsusc.2012.08.094

Yuan, X. J., Chai, Y. Q., Yuan, R., Zhao, Q., & Yang, C. L. (2012). Functionalized graphene oxide-based carbon paste electrode for potentiometric detection of copper ion (II). *Analytical Methods*, *4*(10), 3332–3337. https://doi.org/10.1039/C2AY25674F

Zhang, Z., Xu, F. G., Yang, W. S., Guo, M., Wang, X., Zhang, B., & Tang, J. (2011). A facile one-pot method to high-quality Ag-graphene composite nanosheets for efficient surface-enhanced Raman scattering. *Chemical Communications*, *47*(22), 6440–6442. https://doi.org/10.1039/C1CC11125F

Zhou, Z., He, D. L., Guo, Y. N., Cui, Z., Wang, M., Li, G., & Yang, R. (2009). Fabrication of polyaniline-silver nanocomposites by chronopotentiometry in different ionic liquid microemulsion systems. *Thin Solid Films*, *517*(24), 6767–6771. https://doi.org/10.1016/j.tsf.2009.05.043

Zuo, P. P., Feng, H. F., Xu, Z. Z., Zhang, L. F., Zhang, Y. L., Xia, W., & Zhang, W. Q. (2013). Fabrication of biocompatible and mechanically reinforced graphene oxide-chitosan nanocomposite films. *Chemistry Central Journal*, *7*(1), 39. https://doi.org/10.1186/1752-153X-7-39